

<https://doi.org/10.1038/s41524-024-01288-5>

Strain engineering the spin-valley coupling of the R-stacking sliding ferroelectric bilayer 2H-VX₂ (X = S, Se, Te)

Check for updates

Jiayu Ma^{1,2,3}, Xin Luo^{1,2,3} ✉ & Yue Zheng^{1,2,3}

The emergence of magnetic transition metal dichalcogenides has significantly advanced the development of valleytronics due to the spontaneous breaking of time-reversal symmetry and space-inversion symmetry. However, the lack of regulation methods has prevented researchers from exploring their potential applications. Herein, we propose to use strain engineering to control the spin-valley coupling in the sliding ferroelectric bilayer 2H-VX₂ (X = S, Se, Te). Four multiferroic states are constructed by combining the sliding ferroelectricity and antiferromagnetism in the R-stacking bilayer VX₂, where the spin and valley polarizations are coupled together from the layer-dependent spin-polarized band structures. By applying a small external strain or pressure on the out-of-plane van der Waals direction, we predicted that there is an antiferromagnetic to magnetic transition in the bilayer VX₂, leading to the interesting spin-polarized and chiral circularly polarized radiation at K₊ and K₋ valleys, similar to those found in the magnetic monolayer. To comprehend the coupling between various degrees of freedom in these multiferroic systems, we have developed an effective k-p model. This model unveils a linear relationship between the electric polarization generated by interlayer sliding and the energy difference of the valence band maximum at K₊ and K₋ valleys. Thus, providing an alternate method to measure the electric polarization in the sliding ferroelectrics. Based on the strong coupling between the strain, spin-valley, and electric polarization, it is likely to use the strain to control the interesting emerging properties of 2H-VX₂ such as the anomalous valley Hall effect.

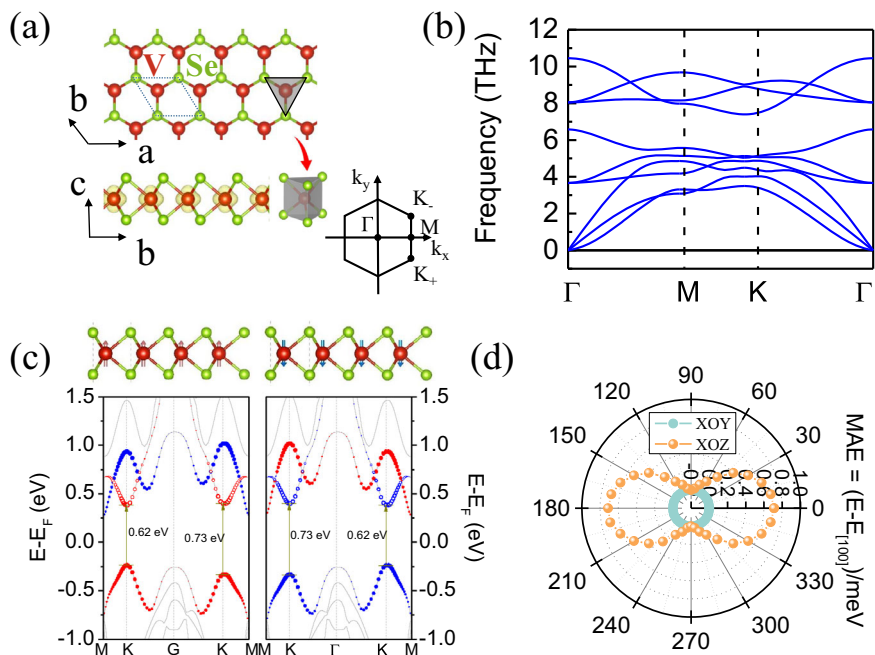
The multiferroic materials, exhibiting coupling among different ferroic orders such as ferroelectricity (FE), ferromagnetism (FM), ferroelasticity, and ferrovalleys (FV), etc., have attracted great interest in recent years due to their promising physical properties and potential applications. The spontaneous ferrovalley polarization¹ is derived in the 2D FM materials when time-reversal symmetry and space central-inversion symmetry are broken. Two prominent multiferroic materials, i.e. BiFeO₃ and TbMnO₃ perovskite oxide compounds^{2,3}, have been extensively studied over the past two decades, for their ability to lower energy consumption and simplify device configuration. Recently, the rapid development of two-dimensional (2D) materials, characterized by increased tunability of physical properties compared to bulk systems due to their weak van der Waals (vdW) interlayer interactions^{4–6} has captured attention in both academic and industry communities. Particularly, the investigation of magnetoelectric

coupling in 2D materials has been emerging as a promising area in electronic device research⁷.

However, the practical applications of 2D FE and 2D FM materials have been greatly limited by their scarcity over the past decades. Only a few 2D FE materials, like In₂Se₃⁸, SnTe⁹, CuInP₂S₆¹⁰, and group-V monolayers (As, Sb, Bi)^{11,12} have been demonstrated in experiments, leaving 2D multiferroic materials even more sparsely explored. Recently, the concept of sliding-ferroelectrics (SFE) is proposed theoretically, by utilizing the weak interlayer vdW interactions of 2D materials^{13–15}. By asymmetrically stacking bilayer 2D materials, a sizable out-of-plane FE polarization can be achieved. This polarization direction can be switched by interlayer sliding between neighboring layers using an external electric field, as confirmed in experimental investigations involving materials such as h-BN^{16,17}, WTe₂¹⁸, β-InSe¹⁹, γ-InSe²⁰, 3R-MoS₂²¹, among others. This proposal shines a light on the construction of 2D multiferroics with

¹Guangdong Provincial Key Laboratory of Magnetoelectric Physics and Devices, School of Physics, Sun Yat-sen University, Guangzhou 510275, China. ²State Key Laboratory of Optoelectronic Materials and Technologies, School of Physics, Sun Yat-sen University, 510275 Guangzhou, China. ³Centre for Physical Mechanics and Biophysics, Sun Yat-Sen University, Guangzhou 510275, China. ✉e-mail: luox77@mail.sysu.edu.cn

Fig. 1 | Ferromagnetic-valley coupling in monolayer VSe₂. **a** The ball-and-stick model and the first Brillouin zone of monolayer 2H-VSe₂. The dashed lines indicate the unit cell and the shallow yellow dotted surface represents the electric density. Phonon dispersion **(b)** and spin-polarized band structures **(c)** of monolayer 2H-VSe₂. The solid 3D arrows located across the V atoms denote the direction of magnetic moments. **d** The magnetocrystalline anisotropy energy (MAE) in XOY and XOZ planes, respectively, where the direction [100] is set as the reference axis.



a different coupling mechanism, which have been implemented in a range of materials including 2H-VSe₂²², 1T-FeCl₂²³, VSi₂P₄²⁴, MnBi₂Te₄²⁵, YI₂²⁶ and MnSe²⁷. The substantial surface-to-volume ratio promotes significant roles for interface engineering and external strain fields in the subtle competition among different ferroic orders in 2D materials. Consequently, external factors like strain²⁸ or electric fields can modulate the coupling among different degrees of freedom—such as electronic charge, spin, and valley—in 2D materials.

In this work, we performed the first-principles calculations on the strain tunable ferroic orders of bilayer R stacking 2D antiferromagnetic VSe₂. Our study reveals that a slight out-of-plane pressure induces antiferromagnetism (AFM) to FM interlayer coupling, significantly influencing the coupling between the spin and valley degree of freedom. More interestingly, the splitting of ferrovalley in energy extrema at K_+ and K_- points of the Brillouin zone shows a linear correlation with interlayer sliding polarization. The strong coupling between the SFE, AFM, and FV allows the mechanical control of ferrovalley as well as the ferromagnetism. This capability holds promise for manipulating exotic physical properties in 2D multiferroics.

Results and discussion

Monolayer properties of VSe₂

As shown in Fig. 1, our calculations show that the single layer 2H-VSe₂ has a ferromagnetic ground state with a magnetic moment of 1 μ_B per V atoms. The absence of the imaginary phonon modes in the phonon dispersion indicates its dynamic stability. 2H-VSe₂, which belongs to the space group of $P\bar{6}m2$, intrinsically breaks the spatial inversion (P-) and time (T-) inversion symmetry, resulting in spontaneous ferrovalley polarization¹. A valley splitting (ΔE) of 0.11 eV and valley polarization is observed at the K_+ and K_- points of the Brillouin zone in the calculated band structures (Fig. 1c). By reversing the direction of the magnetic moment, the bandgap of the two energy valleys in the K_+ and K_- points and valley polarization is reversed accordingly. The magnetocrystalline anisotropy energy (MAE) in the XOY and XOZ planes reveals a preferred magnetization direction in the XOY plane. This coupling between ferrovalley properties and magnetic moment introduces diverse valley physics in R-stacking bilayer antiferromagnetic 2H-VSe₂, which lacks both space and time inversion symmetry simultaneously.

Effect of stackings on ferroelectric properties

As depicted in Fig. 2a–c, there are three different stacking orders for the bilayer VSe₂: AA stacking, AB stacking, and BA stacking. AA stacking belongs to $P\bar{6}m2$ (D_{3H-1}) space group, whose upper layer transitional metal V atoms align to those in the lower layer, resulting in its mirror symmetry M_z . The AB or BA stacking involves a lateral shift of $[\frac{1}{3}, \frac{2}{3}, 0]$ or from AA stacking, thus breaking the M_z symmetry. Bilayer AB stacking VSe₂ belongs to $P3m1$ (C_{3V-1}) space group, with an optimized in-plane lattice constant of 3.32 Å and interlayer vdW gap of 3.12 Å. A sizable out-of-plane dipole moment (D_z) is formed when the interlayer VSe₂ is sliding a short distance from the mirror position between adjacent vdW layers.

Figure 2d–f displays the charge density difference $\Delta\rho$ between the bilayer system and its components for AA, AB, and BA stackings. The plane-average charge density difference in AA stacking reveals a symmetrically distributed charge density, resulting in a zero net interlayer dipole moment. While in AB stacking, a net downward dipole moment (D_\downarrow) of 1.2×10^{-3} C·m⁻² is developed due to the different environment provided by Se atoms around the vdW gap, causing asymmetric distribution of accumulated charge in the out-of-plane direction. A similar analysis is applied to the upward dipole moment (D_\uparrow) in BA stacking. The dipole moments can be easily switched under external electric fields as the structure of AB stacking can slide to one of its three adjacent BA stackings in space under a small field, giving rise to the vdW sliding ferroelectrics.

Figure 3 shows the stacking energy landscape in the unit cell as a function of the lateral shift. The stacking energy is defined as the energy difference between the shifted configuration in a particular stacking order and the AB stacking order. The lateral shift along the [100] direction corresponds to the sliding of one VSe₂ layer along the V-Se bonding direction, while the shift along the $[\bar{1}10]$ direction corresponds to the nearest V-V direction. We note that AB stacking has the lowest stacking energy and degenerates with BA stacking in energy.

Employing the nudged-elastic band (NEB) method, we explored the transition path along the $[\bar{1}10]$ direction. Along this path, an energetically lower transition state than AA (calculated as 134 meV), labeled as ST, is observed. ST corresponds to a fractional lateral shift of $[\frac{1}{2}, \frac{1}{2}, 0]$ with respect to the AA stacking. As shown in Fig. 3c, to switch the dipole

Fig. 2 | The ferroelectric properties of R-stacking VSe₂. The atomic structures (a–c) for AA, AB, and BA stackings of bilayer 2H-VSe₂, respectively. The orange and mint green filling colors represent charge accumulation and depletion respectively. Their planar averaged charge differential density (CDD) along z-direction is displayed in (d–f). The red solid arrows represent the directions of electric polarizations in different stackings.

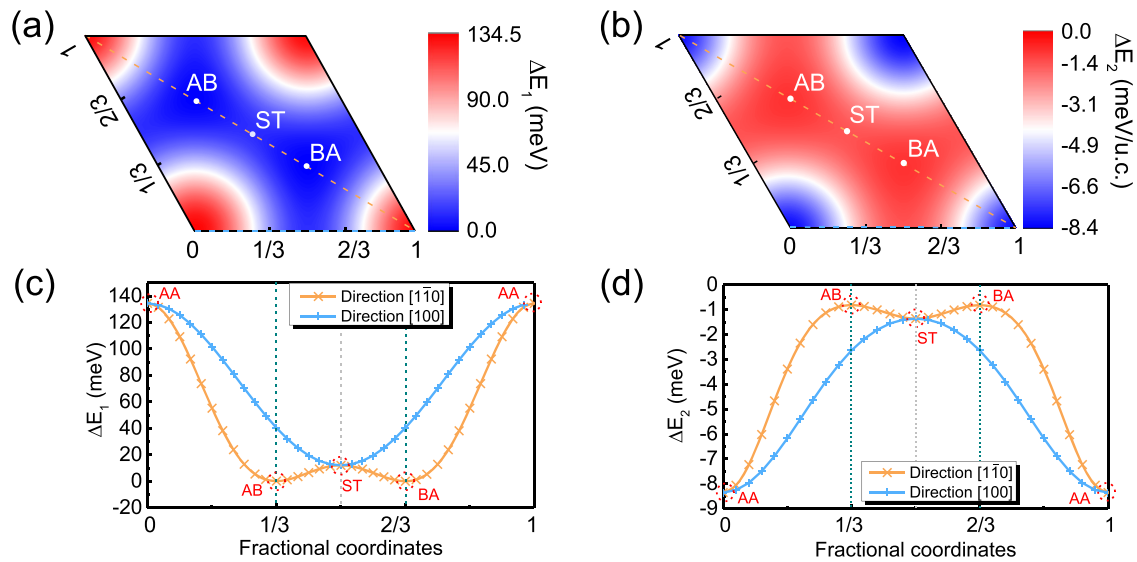
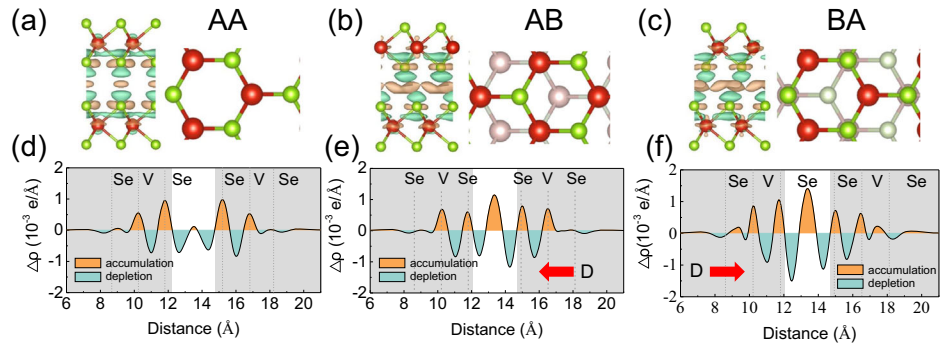


Fig. 3 | Effect of interlayer sliding on energy and magnetic ground state. **a** The energy landscapes of bilayer 2H-VSe₂ while moving the upper layer with respect to the fixed lower layer in real space under the paramagnetic state. **b** The energy

difference between interlayer AFM and FM coupling. **c, d** The energetic profiles along [110] and [100] directions (denoted as orange and blue dashed lines in (a, b)) for (a, b), respectively.

moment from the D_{\downarrow} to D_{\uparrow} by lateral shifting, it needs to overcome a small energy barrier of 9.9 meV per unit cell across the ST point. This barrier is lower compared to the 2D ferroelectric In₂Se₃ (about 66 meV per unit cell)²⁹ and traditional 3D perovskite PbTiO₃ (about 240 meV per unit cell)³⁰, but comparable to h-BN (about 4 meV per unit cell)¹³. This suggests that the polarization in AB stacking bilayer VSe₂ is stable in the ground magnetic state, and the small sliding barrier can be easily overcome by an external electric field, as demonstrated in bilayer h-BN SFE by Wu¹³.

We also calculated the interlayer exchange energy as a function of the lateral shift in Fig. 3b. The interlayer exchange energy is defined as the energy difference between the FM states and interlayer AFM states in bilayer VSe₂. Interestingly, the bilayer VSe₂ prefers the AFM ground state, showing a comparatively lower interlayer exchange energy of -0.82 meV in the AB (BA) stacking. The interlayer exchange energy is much larger in the AA and ST, measuring -8.35 meV and -1.36 meV, respectively. The ultralow exchange energy in the AB stacking also suggests that it could be easily tuned by external field.

Effect of stackings on ferrovalley properties

Combining sliding ferroelectric and interlayer exchange coupling, it could easily create four multiferroic states in bilayer VSe₂, i.e. $D_{\uparrow}M_{\uparrow\downarrow}$, $D_{\downarrow}M_{\uparrow\downarrow}$, $D_{\uparrow}M_{\downarrow\uparrow}$ and $D_{\downarrow}M_{\downarrow\uparrow}$, where $M_{\uparrow\downarrow}$ denotes the magnetic moment of

the top and bottom VSe₂ layer pointing downward and upward. The band structures of $D_{\downarrow}M_{\uparrow\downarrow}$ and $D_{\uparrow}M_{\uparrow\downarrow}$ appear indistinguishable as shown in Fig. 4a and e, so is $D_{\downarrow}M_{\downarrow\uparrow}$ and $D_{\uparrow}M_{\downarrow\uparrow}$. For a particular state featuring both SFE and AFM order, the energy valleys at the adjacent hexagonal Brillouin zone K_{+} and K_{-} no longer remain degenerate due to the breaking of time reversal symmetry and inversion symmetry. The calculated Berry curvatures shown in Fig. 4c and f have opposite signs in value for the K_{+} and K_{-} valleys, suggesting that there are different pseudo-magnetic fields in these valleys. Thus the electrons in adjacent K valley will have an opposite magnetic force and cause the different spin current flow in the top and bottom surface due to the anomalous valley Hall effect. By comparing the electronic structures of different SFE and AFM states in Fig. 4, we found that the band structure is related to Mirror symmetry M_z breaking during sliding, indicating an interconnected relationship between valley polarization and ferroelectric polarization.

There is a strong coupling between spin and valley degree of freedom in the bilayer 2H-VSe₂, as evident in Supplementary Fig. 1, where the V atoms in different layers contribute different energy extrema in the valence band maximum (VBM) and conduction band minimum (CBM). For instance, considering the $D_{\downarrow}M_{\uparrow\downarrow}$ configuration in Fig. 4a, the upper VSe₂ layer contributes the blue spin-down projected band in the CBM while the bottom layer provides the red spin-up projected VBM for AB stacking (also shown in layer resolved band structures in Supplementary

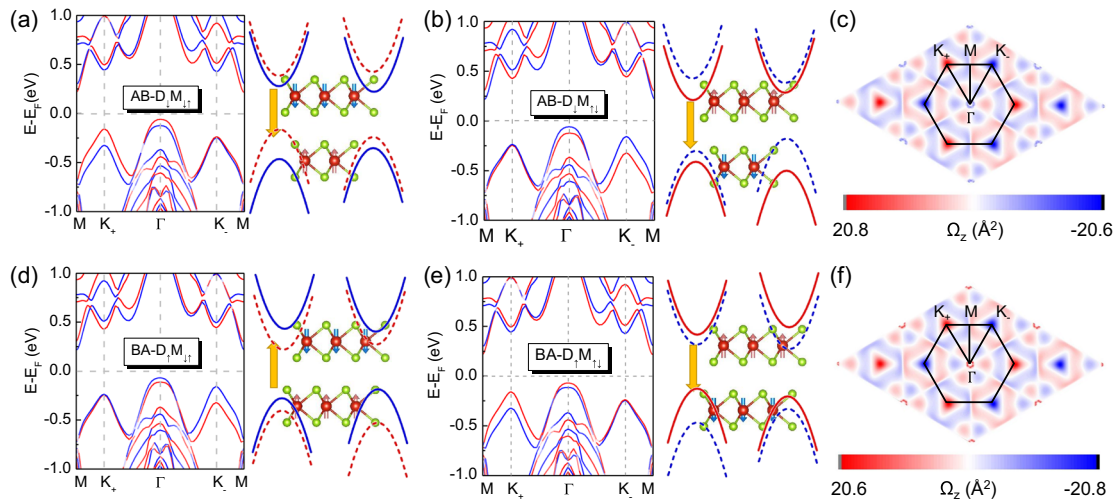


Fig. 4 | Valley polarization properties under different multiferroic couplings. The spin-projected band structures (left panel) and its schematic graph (right panel) of VSe₂ for AB stacking under a head-to-head (a)/tail-to-tail (b) interlayer magnetic moment. Panels d, e is the same conditions for BA stacking. The corresponding calculated Berry curvature for (c) AB stacking and (f) BA stacking in head-to-head AFM configuration. The short dashed and solid lines in the schematic graph represent the contributions from the bottom and upper layer, respectively. The spin-up and spin-down band structures are indicated by red and blue color.

Fig. 5 | Multiferroic properties under different operations. a Electric polarization D variation as a function of interlayer displacement. Red solid line circles the special points mentioned in our context. b Valley split value (U_E) of bilayer 2H-VSe₂ plotted against ferroelectric polarization D and its linear fitted line. The fitting slope is 73.13 eV·m²·C⁻¹. c The transition barrier for AB-BA switching along the direction [110] for VSe₂. d Energy difference $\Delta E_2 = E_{AFM} - E_{FM}$ between interlayer AFM and FM coupling with respect to the c-axis strain (defined as $\frac{c-c_0}{c_0-1}$).

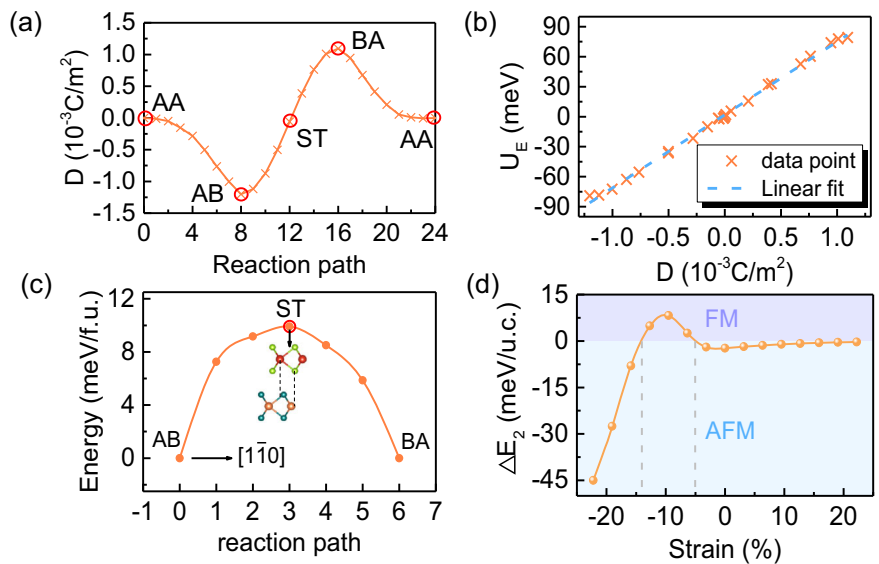


Fig. 1a), confirming the layer-dependent spin polarization^{24,31,32}. While in the K_{\pm} valleys of BA stacking with the $D_{\uparrow}M_{\downarrow\uparrow}$ configuration (Fig. 4c and Supplementary Fig. 1b), the spin-down VBM and spin-up CBM characteristic bands are contributed by upper and bottom layers, respectively. Conversely, in AA stacking, as plotted in Fig. 5c, K_{\pm} valley remain degenerate, exhibiting zero energy difference in the VBM due to the protection of the joint symmetry $\hat{O} \equiv \hat{M}_z \hat{T}$ in space. Furthermore, when the bilayer VSe₂ is in the FM state, the spin-polarized bands do not have layer dependence in the FM state, and the VBM and CBM are mainly contributed from the red spin-up and blue spin-down bands, as shown in Supplementary Fig. 1d-f.

How do the stacking orders and magnetic configurations affect the valley degree of freedom? To answer this question, we enlarged the spin-projected electronic band structures of the $D_{\uparrow}M_{\downarrow\uparrow}$ and $D_{\downarrow}M_{\downarrow\uparrow}$ in Supplementary Fig. 2a and b, where the $M_{\downarrow\uparrow}$ AFM bilayer VSe₂ has a “head to head” magnetic moment in each layer. The $D_{\uparrow}M_{\downarrow\uparrow}$ bilayer VSe₂ has a

spin splitting of 81.7 meV and 49.9 meV in the K_{+} and K_{-} valleys for the lowest two CBM, the corresponding values are 6.6 meV and 164.4 meV for the highest two VBM (also shown in Supplementary Fig. 2a, b). While in the $D_{\downarrow}M_{\downarrow\uparrow}$ configuration, the spin splittings have similar values, but in opposite K_{\pm} valleys. However, as shown in Supplementary Fig. 2c, there is no such a spontaneous ferrovalley in the mirror symmetry AA stacking, although it still has the spin dependent K_{\pm} valley degree of freedom. A calculated energy difference (U_E) of 79.1 meV for the VBM between the K_{+} and the K_{-} valley is found in the AB stacking. This energy difference between the VBM positions in K_{+} and K_{-} valley is comparable with other monolayer magnetic materials, e.g. 105 meV in H-FeCl₂³³, 95 meV in ScI₂³⁴, and 156 meV in NbS₂³⁵, but is considerably large compared with other bilayer systems such as bilayer T-FeCl₂ (4.7 meV)²³ and bilayer YI₂ (24 meV)²⁶. The direction of the dipole polarization can influence the energy extrema of VBM at the K valleys, we depicted the corresponding valence band alignment schematically in Fig. 4 for the AB

and BA stacking orders. Therefore, the layer-dependent spin-polarized band structure can be readily modulated by sliding ferroelectric orders. Since the valley degree of freedom can be detected by the circular polarized light, the spin polarization, polarized photon, and ferroelectric polarizations are related to each other in the multiferroic bilayer VSe₂. Notably when the AB stacking bilayer VSe₂ is in the FM states (Supplementary Fig. 2d), the ferrovalley remains with valley splitting of 9.4 meV between the K₊ and K₋ points. However, different from the monolayer FM VSe₂, the VBM is located at Γ point with a much smaller bandgap of 0.034 eV (Γ to M) in bilayer FM VSe₂.

k-p model analysis

To quantitatively analyze the influence of sliding polarizations on the ferrovalley and spin polarization, we employ an effective k-p model to discuss the interactions of different degrees of freedom in the model by partitioning their effect on the spin-polarized electronic band structures. The effective Hamiltonian of bilayer VSe₂ can be expressed as

$$H_k = I_2 \otimes \begin{bmatrix} H_k^u & H_{\perp} \\ H_{\perp} & H_k^b \end{bmatrix} \quad (1)$$

Here, I₂ is a 2 × 2 identity matrix. H_⊥ represents the interlayer hopping term, which is ignored in our analysis due to the weak vdW interaction. H_k^{u(b)} represents the Hamiltonian of the upper (bottom) layer. This model comprises the nearest hopping term, spin-orbit coupling (SOC), exchange interaction, and electric polarization arising from interlayer sliding:

$$H_k^u = \begin{bmatrix} \frac{\Delta}{2} + \varepsilon + \tau s \lambda_c - s m_c + \frac{U_E}{2} & t_{12}(\tau q_x - i q_y) \\ t_{12}(\tau q_x + i q_y) & -\frac{\Delta}{2} + \varepsilon + \tau s \lambda_v - s m_v + \frac{U_E}{2} \end{bmatrix} \quad (2)$$

$$H_k^b = \begin{bmatrix} \frac{\Delta}{2} + \varepsilon + \tau s \lambda_c + s m_c - \frac{U_E}{2} & t_{12}(\tau q_x - i q_y) \\ t_{12}(\tau q_x + i q_y) & -\frac{\Delta}{2} + \varepsilon + \tau s \lambda_v + s m_v - \frac{U_E}{2} \end{bmatrix} \quad (3)$$

Where Δ represents the band gap at K₊ (K₋) valley, ε is the energy correction related to the fermi level, τ = ± 1 is the valley index, t is an effective nearest-neighbor hopping integral, and **q** = **k** - **K** denotes the relative momentum vector with respect to the K₊ (K₋) valley. s = ± 1 is the spin index where its sign represents spin-up and spin-down respectively. λ_{c(v)} = E_{c(v)↑} - E_{c(v)↓} is the spin splitting at CBM (VBM) in the single-layer TMDs derived from SOC effect. m_{c(v)} = E_{c(v)↓} - E_{c(v)↑} is the spin splitting at CBM (VBM) in the single layer TMDs due to exchange interaction, and U_E is the induced dipole energy of each layer derived from the interlayer charge transfer. For the D_↑M_{v↑} configuration, the corresponding eigenvalues are obtained by performing diagonalization operations on the Hamiltonian:

$$E(\psi_u^{\pm}) = \frac{1}{2} \left[2\varepsilon - \tau(\lambda_c + \lambda_v) + (m_c + m_v) \pm \sqrt{(\Delta'_u)^2 + 4t_{12}^2(\tau^2 q_x^2 + q_y^2)} \right] + \frac{U_E}{2}$$

$$E(\psi_b^{\pm}) = \frac{1}{2} \left[2\varepsilon + \tau(\lambda_c + \lambda_v) + (m_c + m_v) \pm \sqrt{(\Delta'_b)^2 + 4t_{12}^2(\tau^2 q_x^2 + q_y^2)} \right] - \frac{U_E}{2} \quad (4)$$

Here, the gap parameter Δ'_{u(b)} = Δ - (+)τ(λ_c - λ_v) + (m_c - m_v) reflects the band gap of each sub-band contributed by different layers. We noted that the interlayer sliding can easily modulate the relative energy difference between the two sub-bands. The difference between VBM of the two sub-bands is characterized by U_E, expressed as E(ψ_u[↑]) - E(ψ_b[↑]) = U_E. This indicates that the relative altitude of VBM for spin-up and spin-down can be singly tuned by the out of plane (OOP) polarization associated with the interfacial sliding. Since the CBM of K₊ and K₋ valleys have similar values, so the U_E quantity could be considered as a rough estimation of bandgap difference between K₊ and

Table 1 | Elastic constants

Elastic Constants	C ₁₁	C ₃₃	C ₄₄	C ₆₆	C ₁₂	C ₁₃
VS ₂	180.3	54.5	13.7	64.6	51.1	17.2
VSe ₂	137.7	44.6	18.3	63.1	13.5	46.6
VTe ₂	100.7	76.7	15.3	36.4	27.9	28.0

The elastic constants for VS₂, VSe₂, and VTe₂. The unit is in GPa.

K₋ valleys. It's noteworthy that the OOP polarization does not affect the shapes of the band structures. Referring to the band alignment in Fig. 4 (also Supplementary Fig. 2), we can define the direction of valley polarization based on the sign of U_E. The switching from positive to negative valley polarization can be realized by interlayer sliding along the direction [2/3, -2/3, 0] or [-2/3, 2/3, 0]. By comparing the band structures in D_↑M_{v↑}, D_↓M_{v↑}, D_↑M_{v↓} and D_↓M_{v↓} states in Fig. 4, it becomes evident that external fields such as shear sliding, electric field, or magnetic field can be exerted to realize a “four-state switching” between different arrangements of valley polarization and SFE polarization, rendering a ferroelectricity-valley coupling.

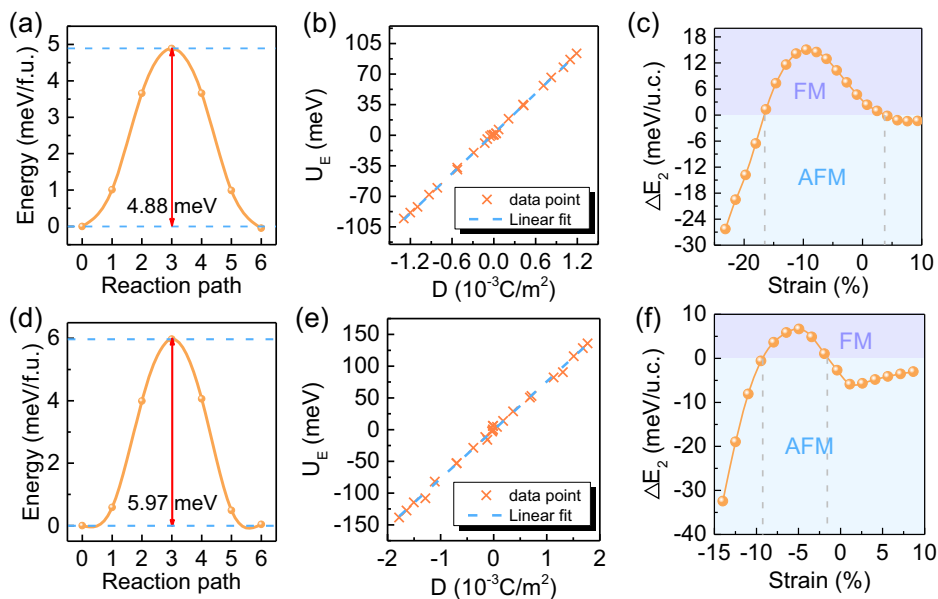
Different means of modulations

The interlayer sliding plays a dual role in directing the electric and valley polarizations simultaneously. Our k-p model reveals a link between the difference in valley VBM at K₊ and K₋ and the interlayer electric polarization. In Fig. 5a, the induced electric dipole polarization is displayed as a function of interlayer displacement during the sliding ferroelectric transition. The electric polarization shows a centrosymmetric tendency with a zero polarization point located at the saddle point ST, whose transition barrier and atomic structure are shown in Fig. 5c. Interestingly, we also calculated the energy difference of the VBM at K₊ and K₋ valleys as a function of the sliding displacement, which shows a similar tendency to the electric polarization. Figure 5c plots the scatter diagram of the energy difference value between K₊ and K₋ valleys U_E with respect to the electric polarization. The fitted function shows that the U_E is linearly related to the electric polarization with a slope factor of 73.13 eV·m²·C⁻¹. This indicates a strong coupling between interlayer electric polarizations and valley polarizations in the SFE bilayer AFM 2H-VSe₂. Furthermore, as depicted in Fig. 3d, there is a giant magneto-electric coupling in the AB stacking bilayer 2H-VSe₂ due to the small interlayer exchange energy. The magnetism can be easily controlled by external fields such as strain or magnetic field. The plot in Fig. 5d demonstrates the interlayer strain-dependent magnetic orders for 2H-VSe₂, where the interlayer AFM ground state switches to the FM ground states under a 5.07% compressive strain. Based on the calculated elastic constants of C₃₃ in Table 1, a small pressure of 3.2 Gpa is sufficient to induce the AFM to FM transition in bilayer 2H-VSe₂, leading to completely different valley responses shown in Supplementary Fig. 2. It is also noted that there is a semiconductor to metal transition when the compressive strain is gradually increased in the bilayer 2H-VSe₂, as shown in Supplementary Fig. 5.

Other candidate materials and outlooks

Our approach can extend to other 2D VX₂ (X = S, Te) magnetic bilayer materials. By replacing the Se element with Te and S element, we show that VTe₂ and VS₂ also exist similar linear ferroelectricity-valley coupling as observed in VSe₂, suggesting the potential for simultaneous SFE and valley polarization switching. As shown in Fig. 6a and c, the switching barriers during the same sliding path for VS₂ and VTe₂ are 4.88 and 5.97 meV, respectively. Figure 6b and c exhibit the scatter diagrams for the valence band energy difference (U_E) between K₊ and K₋ valley as a function of the electric polarizations **D**. The ratio α of U_E to **D** shows similar values across VSe₂, VS₂, and VTe₂. Their optimized structure parameters, ferroelectric polarization, valley splitting and U_E

Fig. 6 | Multiferroic properties in VS₂ and VTe₂. The energy barrier of electric polarization switching for VS₂ (a) and VTe₂ (d) in the direction [110]. b, e Corresponding scatter diagrams and its linear fitting for U_E-D relationship. Energy difference ΔE₂ = E_{AFM}-E_{FM} between interlayer AFM and FM coupling with respect to the c-axis strain for VS₂ (c) and VTe₂ (f).



are listed in Table 2. There exist slight differences in polarization values due to varying charge redistributions among systems. Besides, the electronic band structures under different interlayer AFM configurations ensure the “four state switching”^{22,26}, as shown in the Supplementary Fig. 3 and 4. The strong linear correlation between U_E and electric polarization also provides an alternative method to measure tiny SFE polarization by chiral circularly polarized light. Similar to VS₂, the bilayer VTe₂ also has an AFM ground state, and a compressive strain of 1.8% can cause the transition from AFM to FM, as shown in Fig. 6f. In contrast, the bilayer VS₂ has the FM ground state (Fig. 6c). Based on the calculated elastic constants for VS₂ and VTe₂ in Table 1, predictions suggest the critical strain for the AFM to FM transition in bilayer VS₂ and VTe₂ to be -2.02 GPa (where a negative sign implies tensile strain) and 1.20 GPa, respectively. Based on the above strain-induced AFM to FM phase transition, a multiple external field tunable spin valve device is proposed in Fig. 7. The bilayer AFM 2H-VSe₂ is placed inside a transparent diamond anvil, which could allow the circularly polarized light to penetrate through the anvil. There are both spin-up and spin-down electrons excited under different polarized light when there is no strain, and the flow of spin electrons results in the different spin currents on the left and right edges due the anomalous valley Hall effect. Once the AFM to FM phase transition is induced by an external strain, only one kind of spin current is generated by the polarized light as both K₊ and K₋ valleys generate the same spin electrons. So it could be used to generate different spin currents by the strain engineering. Additionally, applying gate voltage can also induce valley polarization switching, as shown in Fig. 4a

and d, which can also be used to switch the flow direction of spin currents.

In conclusion, based on first-principles density functional theory calculation and the effective k-p model, we unveiled the intrinsic coupling between the ferrovalley and the sliding ferroelectric polarizations in bilayer AFM 2H-VSe₂. The bilayer AFM VSe₂ exhibits a layer-dependent spin-polarized band structure, resulting in an energy difference between the VBM in K₊ and K₋ valleys. The breaking of mirror symmetry plays a critical role in the valley-electric polarization coupling, where dipole polarization and valley polarization arise spontaneously from interlayer sliding. Our DFT calculations highlight a strong linear relationship between the energy difference of VBM among different K valleys and electric polarization, offering a means to measure electric polarization. Similar phenomena were observed in VX₂ (X = S and Te) compounds. The robust coupling between strain, ferromagnetic orders, electric, and valley polarization enables the manipulation of functional properties in bilayer VX₂ systems through strain engineering, promising the design of multifunctional devices.

Methods

Electronic structure calculations

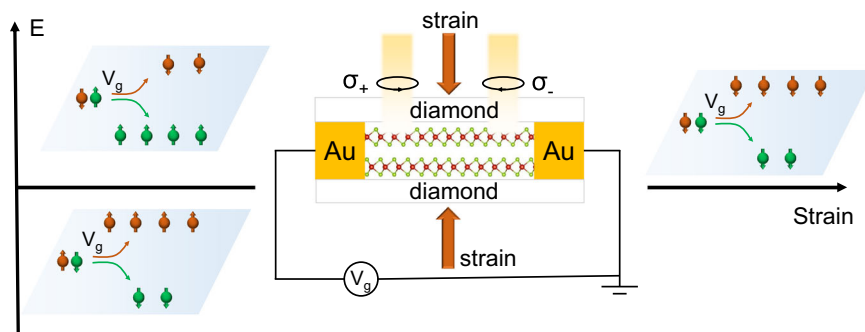
The first-principles density functional theory (DFT) calculations were carried out in the projector augmented wave method³⁶ via the Vienna ab initio simulation package (VASP)^{37,38}. The exchange-correlation function was described by the generalized gradient approximation (GGA) within the Perdew-Burke-Ernzerhof (PBE) formalism³⁹. Structures were considered as fully relaxed when the maximum force between atoms is less than 0.01 eV Å⁻¹ and an energy cutoff of 500 eV was used for the plane wave expansion. The first Brillouin zone was sampled by a Γ-centered Monkhorst-Pack k-point mesh of 15 × 15 × 1. The strong correlation effect of the d electron of V atoms was considered via the on-site Hubbard correction PBE + U method⁴⁰ with the effective U = 1.0 eV⁴¹ in the structural optimization and electronic self-consistent calculation. The vacuum space of 20 Å was introduced to avoid interactions between the adjacent slabs. DFT-D3 method was used to consider the van der Waals correction in all of our bilayer VX₂. The phonon dispersion over a 4 × 4 × 1 supercells were calculated in VASP through PHONOPY package^{42,43} using harmonic approximation.

Table 2 | Parameters for multiferroic coupling

System	a (Å)	D (10 ⁻³ C·m ⁻²)	D (10 ⁻¹² C·m ⁻¹)	U _E (meV)	ΔE (meV)	α (eV·m ² ·C ⁻¹)
VS ₂	3.16	-1.29	-1.34	-95.4	-58.0	76.29
VSe ₂	3.33	-1.20	-1.32	-79.1	-94.9	73.13
VTe ₂	3.53	-1.78	-2.09	-138.3	-122.9	76.39

The lattice constant a, electric dipole moment D and valley split value U_E and fitted coefficient α for VX₂ (X = S, Se, and Te) in AB stacking. ΔE is the bandgap difference between the K₊ and K₋.

Fig. 7 | Strain-tunable spin valve device. The Spin valve devices are designed by manipulating strain and gate voltage to control valley polarization and the flow of spin current.



Data availability

The data that support the findings of the work is in the manuscript's main text and Supplementary Information. Additional data are available from the corresponding author upon request.

Code availability

The central codes used in this paper are VASP. <https://doi.org/10.1103/PhysRevB.47.558>.

Received: 18 January 2024; Accepted: 24 April 2024;

Published online: 10 May 2024

References

- Tong, W., Gong, S., Wan, X. & Duan, C. Concepts of ferrovalley material and anomalous valley Hall effect. *Nat. Commun.* **7**, 1–7 (2016).
- Wang, J. et al. Epitaxial BiFeO₃ multiferroic thin film heterostructures. *Science* **299**, 1719–1722 (2003).
- Kimura, T. et al. Magnetic control of ferroelectric polarization. *Nature* **426**, 55–58 (2003).
- Xu, B., Deng, J., Ding, X., Sun, J. & Liu, J. Z. Van der Waals force-induced intralayer ferroelectric-to-antiferroelectric transition via interlayer sliding in bilayer group-IV monochalcogenides. *npj Comput. Mater.* **8**, 47 (2022).
- Yang, S. et al. Strain-dependent band splitting and spin-flip dynamics in monolayer WS₂. *Nano Lett.* **23**, 3070–3077 (2023).
- Huang, B. et al. Electrical control of 2D magnetism in bilayer CrI₃. *Nat. Nanotechnol.* **13**, 544–548 (2018).
- Gao, Y., Gao, M. & Lu, Y. Two-dimensional multiferroics. *Nanoscale* **13**, 19324–19340 (2021).
- Zhou, Y. et al. Out-of-plane piezoelectricity and ferroelectricity in layered α-In₂Se₃ nanoflakes. *Nano Lett.* **17**, 5508–5513 (2017).
- Chang, K. et al. Discovery of robust in-plane ferroelectricity in atomic-thick SnTe. *Science* **353**, 274–278 (2016).
- Liu, F. et al. Room-temperature ferroelectricity in CuInP₂S₆ ultrathin flakes. *Nat. Commun.* **7**, 12357 (2016).
- Gou, J. et al. Two-dimensional ferroelectricity in a single-element bismuth monolayer. *Nature* **617**, 67 (2023).
- Xiao, C. et al. Elemental ferroelectricity and antiferroelectricity in Group-V monolayer. *Adv. Funct. Mater.* **28**, 1707383 (2018).
- Li, L. & Wu, M. Binary compound bilayer and multilayer with vertical polarizations: Two-dimensional ferroelectrics, multiferroics, and nanogenerators. *ACS Nano* **11**, 6382–6388 (2017).
- Yang, Q., Wu, M. & Li, J. Origin of two-dimensional vertical ferroelectricity in WT_e₂ bilayer and multilayer. *J. Phys. Chem. Lett.* **9**, 7160–7164 (2018).
- Yang, L. & Wu, M. Across-layer sliding ferroelectricity in 2D heterolayers. *Adv. Funct. Mater.* **33**, 2301105 (2023).
- Vizner Stern, M. et al. Interfacial ferroelectricity by van der Waals sliding. *Science* **372**, 1462–1466 (2021).
- Yasuda, K., Wang, X., Watanabe, K., Taniguchi, T. & Jarillo-Herrero, P. Stacking-engineered ferroelectricity in bilayer boron nitride. *Science* **372**, 1458–1462 (2021).
- Fei, Z. et al. Ferroelectric switching of a two-dimensional metal. *Nature* **560**, 336–339 (2018).
- Hu, H. et al. Room-temperature out-of-plane and in-plane ferroelectricity of two-dimensional β-InSe nanoflakes. *Appl. Phys. Lett.* **114**, 252903 (2019).
- Sui, F. et al. Sliding ferroelectricity in van der Waals layered γ-InSe semiconductor. *Nat. Commun.* **14**, 36 (2023).
- Meng, P. et al. Sliding induced multiple polarization states in two-dimensional ferroelectrics. *Nat. Commun.* **13**, 7696 (2022).
- Liu, X., Pyatakov, A. P. & Ren, W. Magnetoelectric coupling in multiferroic bilayer VS₂. *Phys. Rev. Lett.* **125**, 247601 (2020).
- Zhang, T., Xu, X., Huang, B., Dai, Y. & Ma, Y. 2D spontaneous valley polarization from inversion symmetric single-layer lattices. *npj Comput. Mater.* **8**, 64 (2022).
- Zhang, T. et al. Layer-polarized anomalous Hall effects in valleytronic van der Waals bilayers. *Mater. Horiz.* **10**, 483–490 (2022).
- Peng, R. et al. Intrinsic layer-polarized anomalous Hall effect in bilayer MnBi₂Te₄. *Phys. Rev. B* **107**, 085411 (2023).
- Wu, Y. et al. Coexisting ferroelectric and ferrovalley polarizations in bilayer stacked magnetic semiconductors. *Nano Lett.* **23**, 6226–6232 (2023).
- Liu, K., Ma, X., Xu, S., Li, Y. & Zhao, M. Tunable sliding ferroelectricity and magnetoelectric coupling in two-dimensional multiferroic MnSe materials. *npj Comput. Mater.* **9**, 16 (2023).
- Wang, Y., Wang, S., Lu, Y., Jiang, J. & Yang, S. A. Strain-induced isostructural and magnetic phase transitions in monolayer MoN₂. *Nano Lett.* **16**, 4576–4582 (2016).
- Ding, W. et al. Prediction of intrinsic two-dimensional ferroelectrics in In₂Se₃ and other III₂-VI₃ van der Waals materials. *Nat. Commun.* **8**, 14956 (2017).
- Lee, H. J. et al. Scale-free ferroelectricity induced by flat phonon bands in HfO₂. *Science* **369**, 1343–1347 (2020).
- Gao, A. et al. Layer Hall effect in a 2D topological axion antiferromagnet. *Nature* **595**, 521–525 (2021).
- Yu, Z. M., Guan, S., Sheng, X. L., Gao, W. & Yang, S. A. Valley-layer coupling: A new design principle for valleytronics. *Phys. Rev. Lett.* **124**, 037701 (2020).
- Hu, H., Tong, W. Y., Shen, Y. H., Wan, X. & Duan, C. G. Concepts of the half-valley-metal and quantum anomalous valley Hall effect. *npj Comput. Mater.* **6**, 129 (2020).
- Wu, Y. et al. Realizing spontaneous valley polarization and topological phase transitions in monolayer ScX₂ (X = Cl, Br, I). *Acta Mater.* **246**, 118731 (2023).

35. Zang, Y. et al. Large valley-polarized state in single-layer NbX₂ (X = S, Se): Theoretical prediction. *Nano Res.* **14**, 834–839 (2021).
36. Kresse, G. & Joubert, D. From ultrasoft pseudopotentials to the projector augmented-wave method. *Phys. Rev. B* **59**, 1758–1775 (1999).
37. Kresse, G. & Furthmüller, J. Efficient iterative schemes for ab initio total-energy calculations using a plane-wave basis set. *Phys. Rev. B* **54**, 11169–11186 (1996).
38. Kresse, G. & Furthmüller, J. Efficiency of ab-initio total energy calculations for metals and semiconductors using a plane-wave basis set. *Comput. Mater. Sci.* **6**, 15–50 (1996).
39. Perdew, J. P., Burke, K. & Ernzerhof, M. Generalized gradient approximation made simple. *Phys. Rev. Lett.* **77**, 3865–3868 (1996).
40. Liechtenstein, A. I., Anisimov, V. I. & Zaanen, J. Density-functional theory and strong interactions: Orbital ordering in Mott-Hubbard insulators. *Phys. Rev. B* **52**, R5467–R5470 (1995).
41. Esters, M., Hennig, R. G. & Johnson, D. C. Dynamic instabilities in strongly correlated VSe₂ monolayers and bilayers. *Phys. Rev. B* **96**, 235147 (2017).
42. Togo, A., Chaput, L., Tadano, T. & Tanaka, I. Implementation strategies in phonopy and phono3py. *J. Phys. Condens. Matter* **35**, 353001 (2023).
43. Togo, A. First-principles phonon calculations with phonopy and phono3py. *J. Phys. Soc. Jpn.* **92**, 012001 (2023).

Acknowledgements

The authors thank helpful discussions from Prof. H. Wen, Prof. W. Zhu, and Prof. W. Chen. The authors acknowledge support by the Grants from National Natural Science Foundation of China (Nos. 12172386, 12132020), the National Natural Science Foundation of Guangdong Province, China (No. 2021B1515020021), and the Guangdong Provincial Key Laboratory of Magnetoelectric Physics and Devices (No. 2022B1212010008). DFT calculations were performed using the Computational resource of the Centre for Physical Mechanics and Biophysics in the School of Physics at Sun Yat-sen University.

Author contributions

X.L. designed the idea of the research. J.M. performed the first-principles calculations and wrote the manuscript. All the authors contributed to the general discussion, review and editing. X.L and Y.Z. supervised the research.

Competing interests

The authors declare no competing interests.

Additional information

Supplementary information The online version contains supplementary material available at <https://doi.org/10.1038/s41524-024-01288-5>.

Correspondence and requests for materials should be addressed to Xin Luo.

Reprints and permissions information is available at <http://www.nature.com/reprints>

Publisher's note Springer Nature remains neutral with regard to jurisdictional claims in published maps and institutional affiliations.

Open Access This article is licensed under a Creative Commons Attribution 4.0 International License, which permits use, sharing, adaptation, distribution and reproduction in any medium or format, as long as you give appropriate credit to the original author(s) and the source, provide a link to the Creative Commons licence, and indicate if changes were made. The images or other third party material in this article are included in the article's Creative Commons licence, unless indicated otherwise in a credit line to the material. If material is not included in the article's Creative Commons licence and your intended use is not permitted by statutory regulation or exceeds the permitted use, you will need to obtain permission directly from the copyright holder. To view a copy of this licence, visit <http://creativecommons.org/licenses/by/4.0/>.

© The Author(s) 2024